Int J Adv Manuf Technol (2018) 94:2751–2762
DOI 10.1007/s00170-017-1102-7

ORIGINAL ARTICLE

Experimental investigation on electrical discharge diamond grinding of RB-SiC ceramics

Xiaoshuang Rao[1] · **Feihu Zhang**[1] · **Chen Li**[1] · **Yingjie Li**[2]

Received: 7 May 2017 / Accepted: 12 September 2017 / Published online: 18 September 2017

Abstract The reaction-bonded silicon carbide (RB-SiC) ceramics are very difficult to be machined by conventional techniques. In this work, a hybrid process termed electrical discharge diamond grinding (EDDG) was applied to the precision grinding of RB-SiC ceramics considering its weak electrical conductivity. Focus of investigation was especially placed on the effects of grit sizes and polarities of grinding wheel on the surface quality. The machined surface texture and roughness were measured by confocal scanning laser microscope. The surface texture topography and cross-section profile at different grit sizes and polarities were analyzed. The results show that the dominant state of grinding or EDM decides surface texture of machined surface and consequently affects the surface roughness. The surface morphology and subsurface damage were measured by scanning electron microscopy and energy dispersive spectrometer (EDS). The influence of grit sizes and polarities of grinding wheel was focused on the resolidified zone of the machined surface. The material migration phenomenon was found. The subsurface damage was also analyzed by detecting the polished cross-sections, and the depth of subsurface was determined by analyzing the element distribution with EDS spectrums. At last, the formation mechanism of machined surface and the effects of grit sizes and polarities of grinding wheel on machined surface quality were discussed from the viewpoint of discharge energy based on EDM theory.

Keywords Electrical discharge diamond grinding · RB-SiC ceramics · Surface quality · Material migration

1 Introduction

Nowadays, reaction-bonded silicon carbide (RB-SiC) is expected to be one of the most excellent and feasible materials for space optics because of its advantages in developing lightweight large telescope system [1–3]. RB-SiC is fabricated by infiltrating melted silicon into a green body consisting of carbon and SiC powders, followed by reaction and sintering process at about 1700 K to form new SiC grains [4]. These procedures produce a near 100% dense microstructure consisting of a bonded network of silicon carbide with isolated regions of free silicon comprising 10–30% of the microstructure, resulting in an excellent combination of mechanical and thermal properties [5]. Furthermore, the adavages of low processing temperature and negligible dimensional changes during the process enable it to have good shape capability for large and complex shape parts [6], which is especially suitable for frabrication of large-aperture aspheric mirror. Thus, form machining process of aspheric surface is necessary in frabrication of large-aperture SiC aspheric mirror. Grinding is so far the common machining process to obtain the desired shape.

However, since SiC is harder than most other materials except diamond, the available material for removing of RB-SiC is very limited [7]. Many efforts have been made by previous researchers in machining of RB-SiC with diamond abrasive. Yan et al. [8] and Zhang et al. [9] conducted diamond turning experiments on RB-SiC. A very high material removal rate (MRR) was obtained in this method. However, much

✉ Xiaoshuang Rao
rxs_cug@126.com

[1] School of Mechatronics Engineering, Harbin Institute of Technology, Harbin, China

[2] Key Laboratory of Optical System Advance Manufacturing Technology, Changchun Institute of Optics and Fine Mechanics and Physics, Chinese Academy of Science, Changchun 130033, China

dislodgement of SiC grains was observed on the processed surface. Gopal et al. [10, 11] conducted grinding experiment with diamond wheel to find out the effects of depth of cut, feed rate, and grit size during grinding of SiC. Optimal grinding conditions were obtained for maximization of material removal, suggesting that efficient grinding of high-performance ceramics requires selecting operating parameters to maximize removal rate while controlling surface integrity. In Tam et al.'s [12] work, a two-stage fabrication process was proposed to efficient fabrication of RB-SiC optical components. And their experiments had also been verified the efficiency of the two-stage process over that of traditional grinding/polishing techniques.

Although the MRR of RB-SiC ceramics has been increased in some extent through improving or optimizing experiments, tool-wear still remains to be a problem in its industrial application, especially in frabrication of large-aperture aspheric SiC mirror where processing efficiency and surface accuracy would be heavily affected by grinding wheel wear [13, 14]. Considering the electrical conductivity of RB-SiC ceramics, electrical discharge machining (EDM) is an alternative method to machine this hard ceramic materials. A serial of studies on fabrication of micro-holes in RB-SiC by EDM had been carried out by Liew and his co-workers [4, 15–17]. Clijsters et al. [18] suggested that EDM is an effective alternative comparing to traditional manufacturing process like grinding and applied it to obtain flawless complex shaped RB-SiC components. All the features were within the tolerance and met the required shape and geometry accuracy. However, the efficiency of conventional EDM process is still very low when it is applied to machine, a large surface on a SiC ceramic [19, 20]. As a result, diamond grinding remains the first choice of machining of large-scale SiC ceramic blanks, but consideration of the dressing of grinding wheel must be taken during the process.

Electical discharge diamond grinding (EDDG) that integrates diamond grinding and EDM has been demonstrated continuous in-process dressing of the grinding wheel, as material is eroded from the tool electrode as well [21, 22]. This obviates the need to interrupt machining for dressing the grinding wheel. Owing to this advantage, tremendous efforts have been made to investigate machining preformance of difficult-to-machine material such as cemented carbide [23], titanium alloy [24], advanced ceramic composite (Al_2O_3–SiCw–TiC) [25] and metal matrix composites [26, 27]. Singh et al. [28] found that the combination of electrical discharge machining and diamond face grinding improves the machining performance while machining WC-Co composite and average surface roughness increase with increase of wheel speed and current. Kumar et al. [29] used DOE and ANN to predict wear of grinding wheel in EDDG process. They found that lower pulse current, duty ratio, and grain size should be selected to achieve better surface finish of workpiece. Koshy et al. [23] studied the effects of the current and the pulse on-time of the discharges on MRR and grinding forces. Results indicated that the discharge enhances the grinding performance by effectively declogging the wheel surface in EDDG of cemented carbide. Thus it can been seen, the EDDG process has been recognized as a popular hybrid machining process for machining of difficult-to-machine material as its superiority on decrease of grinding force and blockage of grinding wheel as well as increase of the surface quality.

From the literature review, it is obvious that grinding of RB-SiC ceramics assisted with electrical discharge is viable, but no plausible studies so far were conducted using EDDG process. The main objective of the present work is to study the machinability of RB-SiC ceramics by EDDG. Polarities of grinding wheel and diamond grit sizes were taken to investigate the surface quality. The surface roughness and microstructure on the machined surface were detected by confocal scanning laser microscope and scanning electron microscope, respectively. The impact mechanism of polarities and diamond grit sizes on machining of RB-SiC ceramics by EDDG was analyzed based on the theory of EDM in discussion.

2 Experimental details

2.1 Experimental setup

The experiments were conducted on a precision grinding machine with horizontal spindle FS420LC. In these experiments, a hybrid machining process termed electrical discharge diamond grinding was used. This process combines traditional electrical discharge grinding (EDG) and conventional diamond grinding, schamatically shown in Fig. 1. A pulse power supply HDMD-V with three open gap voltage adjustments of 60, 90, and 120 V was appiled to the process. The dielectric fluid was composed of 6.7% emulsified oil and 93.3% distilled water in volume.

As shown in Fig. 1, an iron-bonded (Fe 87%, Cu 10%, Ni 2%, other elements 1%, thermal conductivity 50W/m × k) diamond-grinding wheel instead of the rotating metal or graphite wheel in the EDG process was used as the tool electrode. The sparks are generated in the gap between the workpiece and iron bond of the grinding wheel. Simutaneously, the diamond grits on the iron bond surface remove the materials by mechanical grinding action. Compared with conventional grinding, electrical sparks generated in EDDG process can soften/melt the workpiece, which is helpful for grinding. On the other hand, electrical sparks have an effect on dressing of the grinding wheel by metal bond erosion and keep the grinding wheel sharp in the process, resulting in increase of material removal rate and surface quality.

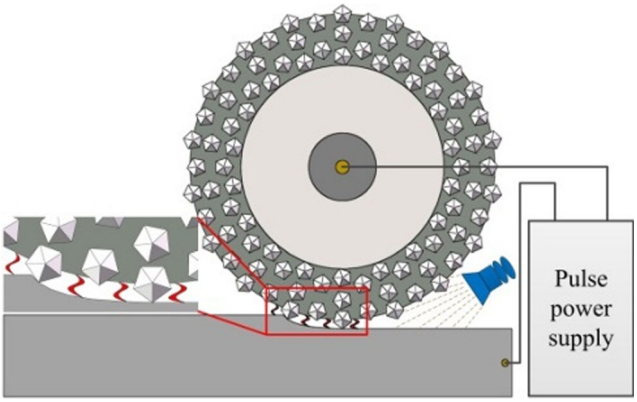

Fig. 1 Schematic diagram of the EDDG process

2.2 Materials

The RB-SiC ceramics employed in the experiments is from Changchun Insitute of Optics, CAS. A microstructure of the RB-SiC ceramic matrix collected by backscattered electron technology of SEM is illustrated in Fig. 2. In the image, elemental contents of given zones were obtained by EDS technology. The results show that the large-size gray particles with average size about 50 μm are raw SiC grains. The white nets around the SiC grains are free Si. Simutaneously, the smaller gray particles among the Si nets are the SiC grains generated from the reaction of Si and C during the infiltration process. What is more, Li et al.'s [30] work collected from XRD pattern further shows the composites of RB-SiC consists of 6H-SiC, 3C-SiC, and Si phases. The as-received samples were cubes with dimensions of 15 mm × 15 mm × 10 mm. Some typical material properties of the samples are shown in Table 1.

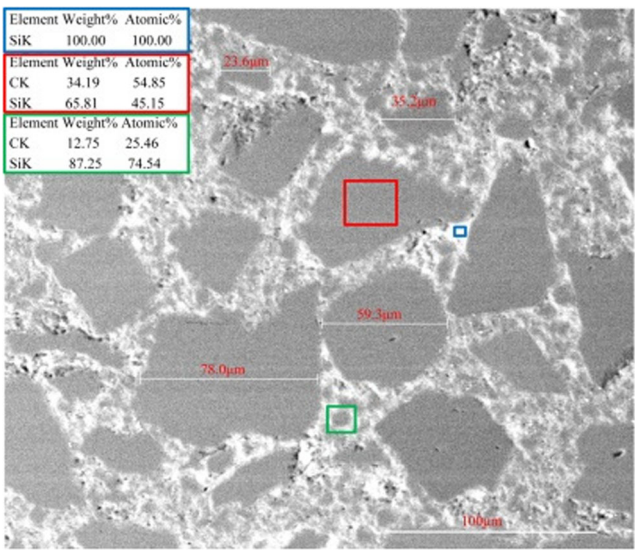

Fig. 2 SEM image of the polished RB-SiC

Table 1 Physical and mechanical properties of RB-SiC ceramics

Property	Values
Density (g/cm^3)	3.0
Young modulus (GPa)	350
Thermal conductivity (W/m × k)	144
Thermal expansion coefficient ($K^{-1} \times 10^{-6}$)	2.4
Electrical resistivity (Ω × cm)	10 [18]
Free Si content (%)	24

Typical material properties of the samples

2.3 Machining conditions and characterization methods

In order to investigate the effects of diamond grit size and metal bonded grinding wheel polarity on surface quality, the experimental parameters were divided into two categories in Table 2. In variables, the situation that the iron-bonded diamond-grinding connected to the positive pole of pulse power supply was marked positive polarity and conversely the negative polarity. The pulse on-time and off-time were chosen 50 μs. The grit sizes of diamond-grinding wheel were selected W40 (grain size about 40 μm), #120 (grain size 106 ~ 125 μm), and #60 (grain size 250 ~ 300 μm). The concentration of diamond grits in the iron bond is 100%.

In these experiments, the effects of electricity parameters on final machined surface quality were evaluated by measuring surface roughness and microstructure of the workpiece on machined surface. The surface roughness with an area of 256 μm × 256 μm (SR Ra) was measured with a confocal scanning laser microscope (CSLM, OLS3000, Japan). Besides, in order to determine the subsurface damage of RB-SiC ceramics mahined by EDDG, the samples were cut in half with diamond wire cutting machine and their cross-sections were polished for 4 h with sand paper (diamond grit size #7000) to eliminate the influence of diamond wire cutting process. Then, the microstructure of the workpiece including machined surface and subsurface was examined with a field emission environment scanning electron microscope (Dual beam FEI Helios Nanolab 600i). The material migration phenomenon on the machined surface was examined by energy dispersion spectrum techniques.

3 Results

3.1 Surface roughness

In order to measure the surface roughness, six observations were done on different positions of the machined surface for each sample. The average of the six assessments was considered as the value of surface roughness. Figure 3 shows 3D surface topography in electrical discharge diamond grinding

Table 2 Design scheme of experimental parameters

Types of parameters	Item	Value
Variables	Polarities	Positive (+): Grinding wheel +, Workpiece –
		Negative (−): Grinding wheel −, Workpiece +
	Grit size	W40, #120, #60
Constants	Gap voltage (V)	120
	Pulse on- and off-time (μs)	50
	Spindle speed (rmp)	2880
	Feed rate (mm/s)	87.8
	Feed depth (μm)	4

In order to investigate the effects of diamond grit size and metal bonded grinding wheel polarity on surface quality, the experimental parameters were divided into two categories

of RB-SiC ceramics influenced by grit sizes and polarities of grinding wheel. It can be seen that, for grit size *W40*, there are more cavities in positive grinding wheel polarity than that in negative polarity on the machined surface, resulting from the action of electrical sparks over diamond grains on the material removal in the EDDG process [31, 32]. But for grit size *#120* and *#60*, the surface textures in the positive polarity situation are smoother and flatter than that in negative polarity situation. The cavities on the machined surface in negative-grinding wheel polarity are deeper and larger than those in positive-

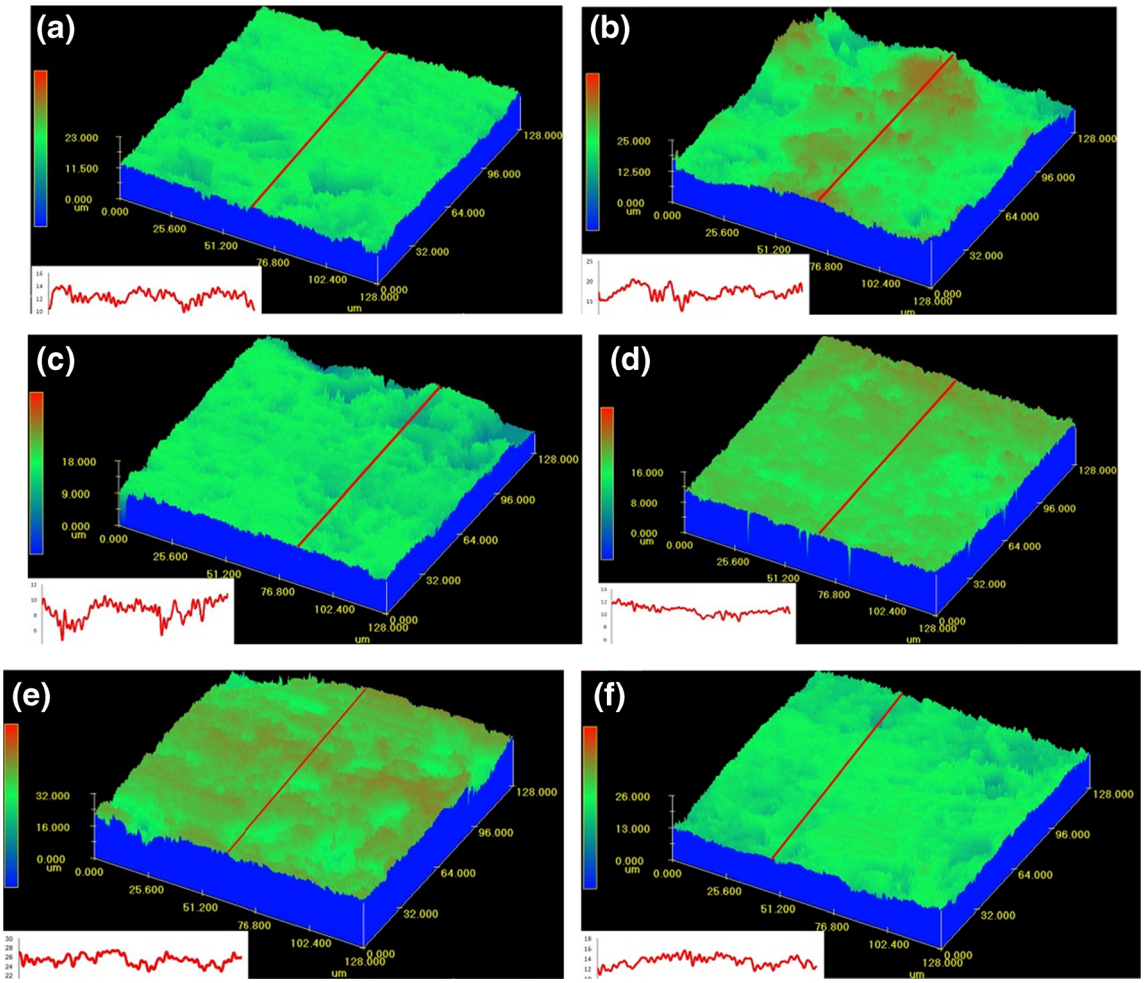

Fig. 3 3D texture models of the machined surface in different grit size and grinding wheel polarity situations **a** grinding wheel "–," grit size *W40* **b** grinding wheel "+," grit size *W40* **c** grinding wheel "–," grit size *#120* **d** grinding wheel "+," grit size *#120* **e** grinding wheel "–," grit size *#60*, and **f** grinding wheel "+," grit size *#60*

grinding wheel polarity, and the extent increases with the increase of the grit sizes. The results indicate that grinding action increases under the situation of large grit size and positive grinding wheel polarity. This is because electrical sparks diminish with the increase of breakdown voltage between the workpiece and grinding wheel.

The lines perpendicular to grit motion descript the waviness of the machined surface, shown in the bottom left corner of Fig. 3. The cross sectional profile in positive-grinding wheel polarity is more irregular as compared to that in negative-grinding wheel polarity for girt size *W40*. And the maximum profile valley depth is larger in positive-grinding wheel polarity. When the girt size is *W40*, there will be a small gap between the iron bond and workpiece; more materials are removed by sparks with high-discharge energy than that by diamond grinding in positive-grinding wheel polarity. But except for grit size *W40*, the cross sectional profiles exhibit smaller peak and valley depths in positive-grinding wheel polarity, which ultimately leads to smaller deviations of the surface roughness in positive-grinding wheel polarity than that in negative-grinding wheel polarity (Fig. 4). With the increase of grit size, the protrusion of diamond grit increases the interelectrode gap in the EDDG process. The sparks diminish owing to increase the corresponding breakdown voltage. Besides, when the grinding wheel is connected with the negative polarity of pulse power energy, the breakdown voltage would also increase because of the higher thermal conductivity of RB-SiC material as the positive electrode. The materials on the surface of workpiece removed by diamond grits in brittle regime gradually increase with the increase of diamond grit size. Thus, the shocks of the cross-sectional profile curves become more and more apparent with the increase of diamond grit size in the same grinding wheel polarity.

The specific values of surface roughness affected by diamond grit sizes and grinding wheel polarities are illustrated in Fig. 4. It is apparent that surface roughness initially decreases and then increases with an increase of the diamond grit size at both two situations of grinding wheel polarity. The surface roughness in positive-grinding wheel polarity is lower than that in negative grinding wheel polarity for both diamond grit sizes *#120* and *#60*. With the increase of grit size, the grinding trace becomes so evident that the surface roughness increases [33]. But for diamond grit size *W40*, the surface roughness is about two times higher in positive-grinding wheel polarity than that in negative-grinding wheel polarity. This is because the ignition of the discharge is initiated more easily in positive grinding wheel polarity, leading to the EDM dominant state. Substantial craters and resolidifications were generated on the machined surface, resulting in a rough surface.

However, it is noteworthy that the surface roughness of the RB-SiC ceramic machined with grit size *W40* is little higher than that with grit size *#120* in negative-grinding wheel polarity. This attributes to smaller interelectrode gap obtained at grit

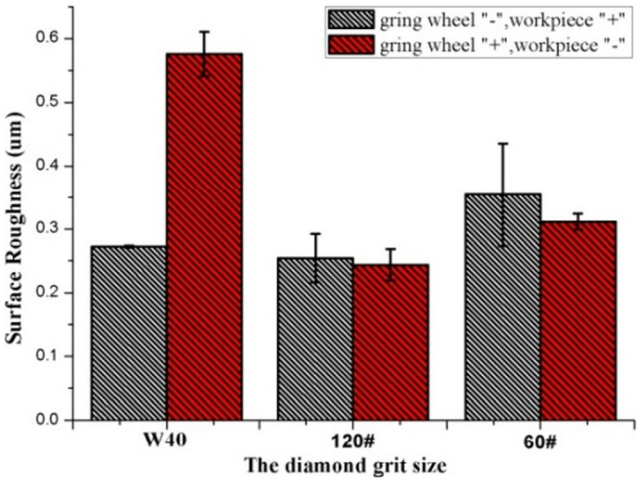

Fig. 4 Surface roughness of different grit sizes and electrode polarities

size *W40*. As diamond grain size of *W40* is smaller than that of *#120*, the breakdown voltage decreases with a small interelectrode gap. The erosion and thermal effect on grinding wheel caused by electrical sparks result in diamond graphitization and pullout, which decreases grinding action on the workpiece and increase surface roughness. This phenomenon has also been reported in reference [34].

3.2 Surface morphology

In the experiments, the finished surface of RB-SiC ceramic machined by EDDG is found charactering with grinding zone and resolidified zone, shown in Fig. 5a. Scratches and resolidified materials are the main features of grinding zone and resolidified zone, respectively. Fig. 5b shows the details of the resolidified zone by enlargement of site "b" in Fig. 5a. It reveals the appearance of scratches, cracks, craters, cavities, and droplets on the machined surface in resolidified zone. Here, it is necessary to note, however, that the scratches induced by diamond grits in resolidified zone are depended on dicharge energy and diamond grit protrusion height, which will be disscused later in more details in disscusion section. In Liew et al.'s [16] study, the white particles, namely droplets, are suggessted as the material migration phenomena. Thus, the EDS technology was also applied in this research to analyzed the elemental composition of the machined surface. Two different locations, grinding region "c" and droplet region "d," were chosen for detection as indicated in Fig. 5b. Fig. 5c and d show the elemental composition and their percentages of the two locations.

As shown in Fig. 5c, the EDS spectrum for grinding region "c" consists of little ferrum (Fe) with 3.77% of weight. This result demonstrates that material migration has happened in EDDG of RB-SiC samples, resulting in ferrum from the iron bond of grinding wheel being detected on the surface of grinding zone. In region "d," ferrum is detected at higher weight

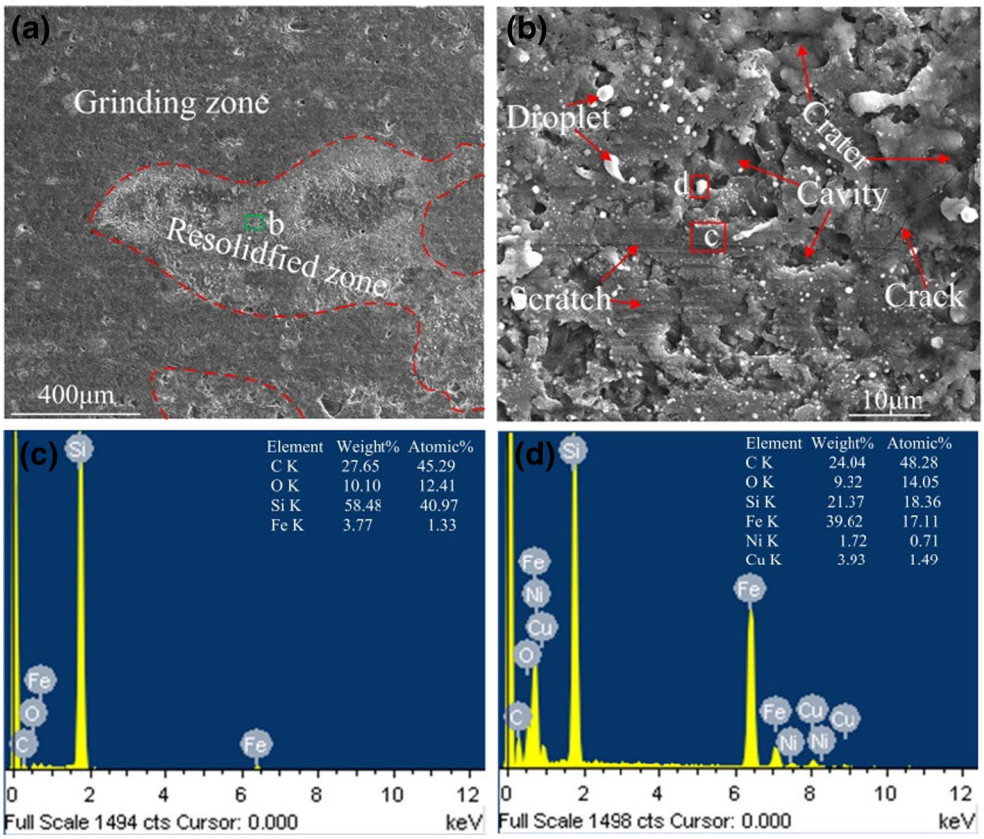

Fig. 5 Surface morphology and EDS analysis of RB-SiC ceramic machined by EDDG

percentage up to 39.62%. Simultaneously, other more impurity elements such as Cu and Ni in iron bond of grinding wheel were also detected, depicted in Fig. 5d. The total weight percentage of metal elements from iron bond is over 45%, which indicated that the particle droplet was formed duo to the melting of iron bond of grinding wheel. It is worthy to note that, however, the elements and their weight percentage are much lower in grinding region than that in droplet region, which indicates that the material migration occured in EDDG process can be removed by diamond grits.

Figure 6 represents SEM micrographs of machined surface focused on resolidified zone that depicted in Fig. 5a, from which the effects of grit sizes and polarities of grinding wheel on machined surface microstructure of RB-SiC ceramics can be studied. It can be seen that grinding traces increase and craters become shallower and smaller with the increase of diamond grit size. For the same diamond grit size, the craters are so shallower in positive-grinding wheel polarity that the resolidified material was removed by subsequent diamond grits to leave obvious stracthes in the resolidified zone. This is because the bombardment by positive ions is weaker than that by electrons, the craters on the workpiece surface produced by positive ions are shallow [33].

It is interesting to find that the grinding traces akin to metal cutting stripes are clearly seen on SiC grains in positive-grinding wheel polarity for finished surface machined with diamond grit size *W40*, which indicates that material removal in ductile regime is possible with help of electrical sparks in precision grinding of RB-SiC ceramics. Compared with main surface characteristics of resolidified materials shown in Fig. 6a, there are more droplets on machined surface of RB-SiC ceramic shown in Fig. 6b, which indicates that anode dissipation is over cathode dissipation. The result is that material migration of iron bond has happened, and droplets are formed in positive-grinding wheel polarity. This is because electrolysis reaction occurs easily in positive tool polarity under the application of the water-based emulsion, and the removed tool material is mostly ionized into metallic ion, which can attach to the workpiece surface easily [35]. Figure 6c and d represent microstructure of machined surface ground with diamond grit size *#120*. A large scale resolidified zone is found with obvious cracks owing to rapid melting/cooling of the workpiece material in negative grinding wheel polarity shown in Fig. 6c. In contrast, when the grinding wheel was in positive polarity, only the resolidified material at the bottom of craters was left, but the surroundings were ground by diamond grits. When the diamond grit size was further increased, say grit size #60 (250 ~ 300 μm), smaller craters were formated and grinding traces increased. Compared with microstructures of craters on the surface in negative-grinding wheel polarity shown in Fig. 6e, the resolidified materials in craters were all almostly removed by diamond grits in

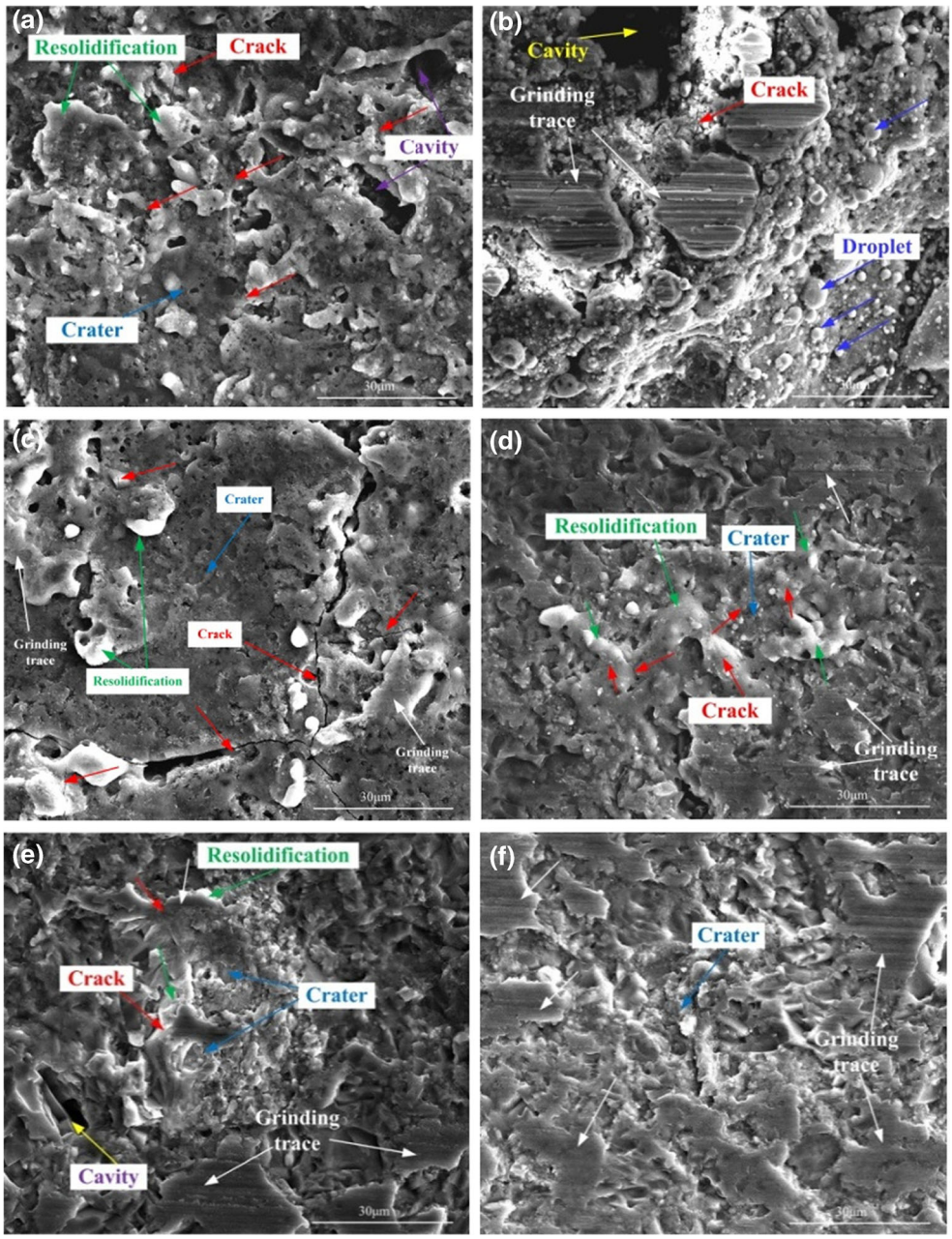

Fig. 6 SEM micrographs of machined surface focused on resolidified zone in different conditions: **a** grinding wheel "–," grit size *W40* **b** grinding wheel "+," grit size *W40* **c** grinding wheel "–," grit size *#120* **d** grinding wheel "+," grit size *#120* **e** grinding wheel "–," grit size *#60*, and **f** grit size *#60*, grinding wheel "+"

positive-grinding wheel polarity as shown in Fig. 6f. This, on one hand, attributes to shallow craters formed by electrical sparks in positive-grinding wheel polarity. On the other hand, with the increase of the diamond grit size, the protrution height of diamond grits on the bond surface of grinding wheel increases enough to remove all resolidified materials in the craters.

3.3 Subsurface damage

In order to examine subsurface damage of RB-SiC ceramic machined by EDDG, detections were taken on cross-sections of the machined surface with combination of SEM and EDS. Figure 7 represents SEM images of the cross-sections of RB-SiC ceramics machined under different grinding wheel polarities and diamond grit sizes in EDDG process. It can be seen that an obvious resolidified layer is covered on the machined surface. In the same grinding wheel polarity, the resolidified layer decreases with the increase of diamond grit size. The reason is that sparks decrease with increase of discharge gap attributing to higher protrution of diamond grit on surface of grinding wheel. And grinding action of larger dimond grits removes more material at same setting cutting depth, resulting in decrease of resolidified layer.

In addition, a heat-affected layer characterized with microcracks, porosities, or samller grains than that in matrix

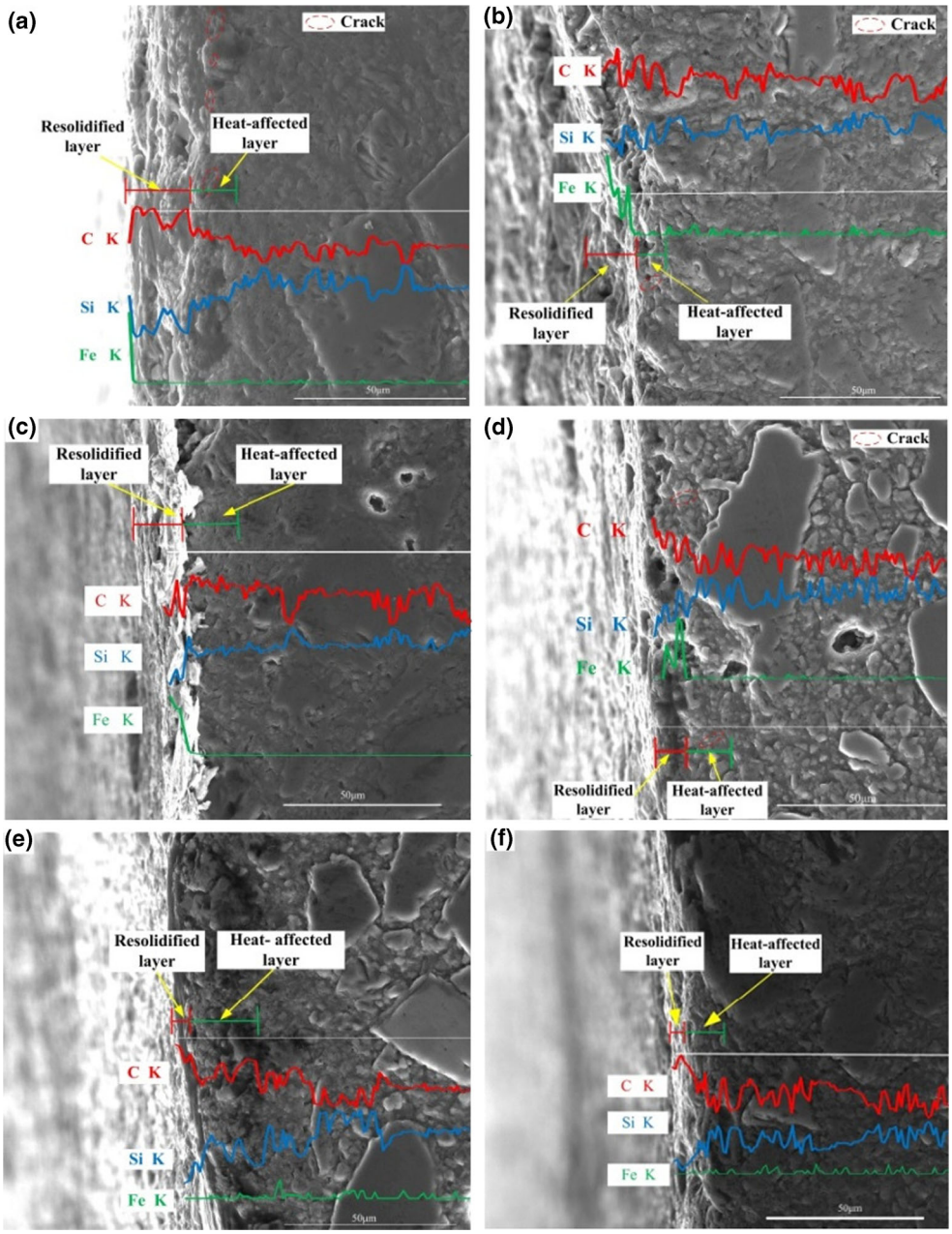

Fig. 7 SEM images of cross-sections of RB-SiC ceramics machined by EDDG at different grit size and grinding wheel polarities situations. **a** grinding wheel "−," grit size *W40* **b** grinding wheel "+," grit size *W40* **c** grinding wheel "−," grit size *#120* **d** grinding wheel "+," grit size *#120* **e** grinding wheel "−," grit size *#60*, and **f** grit size *#60*, grinding wheel "+"

of RB-SiC ceramics is also found beneath the resolidified layer, as reported in reference [18, 34]. Since this layer is close to the machined surface, it is much likely impacted by instant high temperature of electrical sparks. It is interesting that the thickness of heat-affected layer increases with the increase of diamond grit size, which is contrary to that of resolidified layer. This attributes to different amount of heat transferred to the workpiece, which will be specificly discussed in the discusion section. To further comfrim the thickness of the subsurface damage, the elemental concentrations of Fe transferred from iron bond of grinding wheel and C and Si from parent material were measured by a line scan of EDS on cross-sections of the machined surfaces, illustrated in Fig. 7a~f. It can be seen that Fe mainly distributes on/near the machines' surface and reduces with the increase of diamond grit sizes. Furthermore, all elemental concentrations of C are higher than that of the matrix while the opposites are for Si in resolidified layer.

Figure 7a and b show the subsurface damages under the machining condition of grit size *W40*. Compared with the significant changes of the concentrations of C and Si in the resolidified layer in negative-grinding wheel polarity, smaller changes of relative contents of them have been found in positive-grinding wheel polarity. Besides, high concentration of Fe is also detected in both resolidified layer. An uneven surface was formed in positive-grinding wheel polarity

because of the dominate state of EDM in EDDG process. The distributions of elemental concentrations imply that the thicknesses of resolidified layer and heat-affected layer are 19 and 10 μm in negative-grinding wheel polarity and 15 and 8 μm in positive-grinding wheel polarity.

In Fig. 7c, a visible deposition layer is covered on the surface machined with grit size *#120* in negative-grinding wheel polarity. Smaller SiC grains than the matrix are found in heat-affected layer. According to the distributions of elemental concentrations, the thicknesses of resolidified layer and heat-affected layer are determined 15 and 18 μm, respectively. By comparision, a resolidified layer with Fe distribution is detected in positive-grinding wheel polarity, verifying that some of melted iron bond was reacted with or dissolved in the material during the EDDG process [35]. In the heat-affected layer, small SiC grains, porosities, and microcracks are also found. The thicknesses of resolidified layer and heat-affected layer in positive-grinding wheel polarity are 9 and 13 μm, respectively.

For grit size *#60*, a thinner resolidified layer but a thicker heat-affected layer is found on the surface machined by EDDG, depicted in Fig. 7e and f. It is noteworthy that no Fe distributions were detected on the cross-sections of machined surface in both grinding wheel polarities. In negative-grinding wheel polarity, however, small SiC grains and dark zone with higher C content are visible in heat-affected layer. Duo to high temperature is generated by electrical sparks in EDDG process; SiC grains of the matrix are decomposited, and free Si is evaporated to leave voids in the matrix. The EDS spectrums of the elemental concentration show that the thicknesses of resolidified layer and heat-affected layer are 6 and 20 μm in negative-grinding wheel polarity and 5 and 13 μm in positive-grinding wheel polarity, respectively.

4 Discussions

4.1 Formation mechanisms of the machined surface and subsurface damage

As mentioned in section 2.1, the simultaneous influence of diamond grains and electrical sparks causes abrasion and surface melting respectively in EDDG process. Therefore, the workpiece material is removed by the combined effect of electro-erosion and micro-cutting process (mechanical effect of diamond grits) [36]. The detail of machined surface and subsurface damage formation in EDDG of RB-SiC ceramics is illustrated in Fig. 8. It can be seen that electrical sparks leave craters on the surface by melting and vaporization of the free Si because of its higher electrical conductivity than SiC grains [16]. At the same time, deposition is also formed on the surface because melted bond material of grinding wheel caused by sparks is cooled and then resolidified by dielectric fluid.

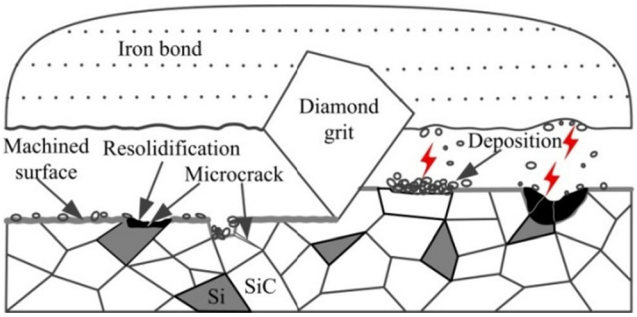

Fig. 8 Detail of machined surface and subsurface damage formation in EDDG of RB-SiC ceramics

Besides, cavities may also appear on the surface due to decrease of bonded strength resulting in pullout of SiC grain under the action of electrical sparks. At last, the diamond grits cut away the matrix and deposition by grinding action in micro-scale. During the EDDG process, the grinding and EDM alternate with each other to form the finished surface of RB-SiC ceramics. Consequently, the final microstructure of the machined surface is depended on the synergetic interaction effect of electro-discharge action and abrasion action.

On the other hand, heat concentration on the surface decomposes partial SiC grains into C and Si. As the melting point of C is higher than that of Si, this heat evaporates the free silicon (~ 3200 °C) among the boundaries of SiC particles and the grown SiC grains which are generated during the infiltration process [18], consequently more C will be left on the surface and subsurface in the EDDG process. The thermal impacts of the sparks also cause a very rapid quench rate of the heated material with the help of emulsion in the resolidified zone. These thermal waves cause expansion and contraction of resolidified and heat-affected material, resulting in the microcracks in resolidified layer [34]. What is more, the diamond grits also have impact on the SiC grains around the cavities. Another form of micro-cracks will initiate at the grain boundary in heat-affected layer because of the decrease of bonded strength. Thus, it can be seen that these subsurface damages are mainly affected by the thermal energy transferred to the workpiece.

4.2 Effects of polarities and grit sizes

During EDDG process, the polarities and grit size of grinding wheel play an important role on surface microstructures and subsurface damages. Specifically, the polarities and grit size of grinding wheel have effects on heat transferred to the workpiece because of different thermal conductivity of electrode and interelectrode gap during the process.

In EDM, the electric breakdown threshold depends on the electrode material [37]. The anode material with low conductivity is easily melted/evaporated by electrical discharge. More ions are generated in the bulk dielectric,

which results in increasing pressure in the gap and finally grows to the breakdown. Thus, anode material with low-thermal conductivity, for example, iron (thermal conductivity is 50W/m × k) rather than RB-SiC ceramic (thermal conductivity is 144W/m × k), will have lower breakdown voltage threshold [38, 39].

The same situation also exists for interelectrode gap. For the same fluid dielectric, the dielectric strength keeps constant so that the breakdown voltage threshold is directly proportional to the interelectrode gap, which is given by the following [39]:

$$U_{\mathrm{kp}} = E_{\mathrm{kp}} l \tag{1}$$

where U_{kp} is the breakdown voltage threshold. E_{kp} is the electric field in the dielectric fluid, which is constant when the interelectrode gap is less than 1 mm. l is the interelectrode gap size. This linear relationship between the breakdown voltage and gap size at micrometer and sub-millimeter separations has been verified by investigations in references [40, 41]. Therefore, the breakdown is more difficult to happen in large interelectrode gap than that in small interelectrode gap. In EDDG process, the interelectrode gap is obtained from the gap between the iron bond surface of grinding wheel and workepiece, which depends on the protrusion height (p_{h}) and cutting depth (h) shown in Fig. 9. The protrusion height was usually suggested about 30% of the grit size [21, 34]. Thus, the interelectrode gap is affected by grit size when the cutting depth keeps constant. The breakdown voltage threshold increases with increase of grit size.

In EDM, the process is the conversion of discharge energy into thermal energy through a series of discrete electrical discharges occurring between the electrode and workpiece immersed in a dielectric fluid [42]. Then the thermal energy dissipates through plasma, cathode, and anode. The material properties of individual electrodes determine the fraction of input heat going into the electrodes. Theoretically, anode with lower thermal diffusivity gets the lower share of the input power than that anode with higher thermal diffusivity [43]. The total discharge energy available to the plasma, cathode, and anode in EDM is given by the following [44]:

$$W = \int_0^{\tau} u(t) i(t) dt \tag{2}$$

where W is discharge energy, $u(t)$ and $i(t)$ are the instantaneous voltage and instantaneous current, respectively, τ is pulse duration. Practically, the electrical discharge is a kind of plasma. As the plasma is in fact a kind of electrically conductive gas with high temperature, the Eq. (2) is also given by the following:

$$W = \int_0^{\tau} E_c(t) \cdot l \cdot i(t) dt \tag{3}$$

where E_{c} (t) is the electric field in the plasma, which is a constant equal to E_{kp}. Therefore, the discharge energy will

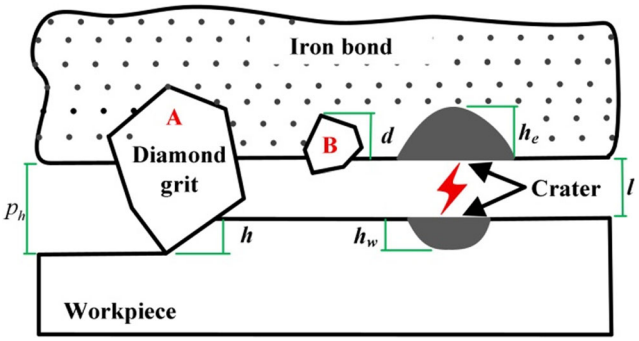

Fig. 9 Relationship of interelectrode gap and protrusion height

increase at large interelectrode gap when the electrical sparks occur, resulting in increase of the power dissipation through cathode and anode. Consequently, a thicker heat-affected layer is formed.

In EDDG process, it can be controlled either in grinding dominant state with a relatively less contribution of electrical erosion to acquire a reduced heat-affected surface layer, or in EDM dominant state with a relatively less contribution of grinding to reduce machining force, or in a well-balanced state between the grinding and the erosion [36]. The varied breakdown voltage changes the dominant state of grinding or EDM in the EDDG process. Due to less sparks occur in rising of breakdown voltage with increase of diamond grit, a thinner resolidified layer consisted of shallow craters and less resolidified material is formed on the machined surface of RB-SiC ceramics. On the other hand, large-size grits remove more resolidified material to leave a thin resolidified layer. Simultaneously, electrical discharge interactions on the metal bond grinding wheel lead to its self-dressing in process. More sparks generate deeper craters on iron bond surface because of its lower thermal conductivity when it is anode. When the diamond grit size is so small (such as grit B shown in Fig. 9, $d < h_{\mathrm{e}}$) that a large number of grits are pulled out by the dressing of electrical sparks, the grinding action is weaker in positive-electrode polarity than that in negative-electrode polarity, which is responsible for the surface roughness and microstructure in positive-grinding wheel polarity being worse than that in negative-grinding wheel polarity.

5 Conclusions

Considering the hardness and conductivity, a hybrid process termed electrical discharge diamond grinding was applied in machining of RB-SiC ceramics in this paper. An extensive analysis has been conducted to investigate the effect of polarity and grit size of grinding wheel on surface roughness, surface morphology, and subsurface damage. The following conclusions can be drawn based on the investigations.

(1) The machined surface represents more smoothness and flatness with a regular cross-sectional profile in positive-grinding wheel polarity than that in negative-grinding wheel polarity except for grit size *W40*. However, the surface deteriorates with increase of grit size because of material removal in brittle regime, resulting in that surface roughness initially decreases and then increases with an increase of diamond grit size in both grinding wheel polarity situations.

(2) The surface of RB-SiC ceramic machined by EDDG consists of grinding zone and resolidified zone, which are mainly characterized with scratches and resolidified material, respectively. Material migration is found in the resolidified zone and has been demonstrated to be removed by subsequent diamond grits.

(3) The grinding traces become apparent and craters become shallow and small because of the outstanding of grinding dominant state with increase of the diamond grit size. For the same grit size, as the bombardment by positive ions is weaker than that by electrons, the craters are also smaller and shallower in positive-grinding wheel polarity than that in negative-grinding wheel polarity.

(4) A resolidified layer and a heat-affected layer are the main subsurface damages of RB-SiC ceramics machined by EDDG. The thickness of resolidified layer decreases with increase of diamond grit sizes. However, it is interesting that the thickness of heat-affected layer increases with the increase of diamond grit sizes, which is contrary to that of resolidified layer. This attributes to more energy transferred to the workpiece in large grit size. The thicknesses of resolidified layer and heat-affected layer were finally determined by analyzing distributions of elemental concentration.

Acknowledgement This work was supported by the National Key Research and Development Program of China (2016YFB1102204) and the National Key Basic Research and Development Program of China (973 program, Grant no. 2011CB013202).

References

1. Yui YY, Kumura T, Tange Y (2004) Development of reaction-sintered SiC mirror for space-borne optics. 5th Int Conf Space Opt 554:673–679
2. Tsuno K, Irikado H, Hamada K, Kazuhiko O, Ishida J, Suyama S, Itoh Y, Ebizuka N, Eto H, Dai Y (2004) Reaction-sintered silicon carbide: newly developed material for lightweight mirrors. 5th Int Conf Space Opt 554:681–685
3. Yui YY, Kimura T, Tange Y (2004) High-strength reaction-sintered SiC: a new candidate material for large spaceborne telescope systems. Proc SPIE 5570:289–300
4. Liew PJ, Yan J, Kuriyagawa T (2013) Carbon nanofiber assisted micro electro discharge machining of reaction-bonded silicon carbide. J Mater Process Technol 213(7):1076–1087
5. Ealey MA, Weaver GQ (1996) Developmental history and trends for reaction bonded silicon carbide mirrors. In Proc SPIE 2857:66–72
6. Zhang G, Zhao R, Zhao W (2007) Fabrication technique of large-scale lightweight SiC space mirror. In 3rd International Symposium on Advanced Optical Manufacturing and Testing Technologies: Large Mirrors and Telescopes. International Society for Optics and Photonics 67210B–67210B
7. Deng H, Yamamura K (2012) Smoothing of reaction sintered silicon carbide using plasma assisted polishing. Curr Appl Phys 12: S24–S28
8. Yan J, Zhang Z, Kuriyagawa T (2009) Mechanism for material removal in diamond turning of reaction-bonded silicon carbide. Int J Mach Tools Manuf 49(5):366–374
9. Zhang Z, Yan J, Kuriyagawa T (2011) Study on tool wear characteristics in diamond turning of reaction-bonded silicon carbide. Int J Adv Manuf Technol 57(1):117–125
10. Gopal AV, Rao PV (2003) Selection of optimum conditions for maximum material removal rate with surface finish and damage as constraints in SiC grinding. Int J Mach Tools Manuf 43(13): 1327–1336
11. Gopal AV, Rao PV (2002) Modeling of grinding of silicon carbide with diamond wheels. Miner Process Extr Metall Rev 23(1):51–63
12. Tam HY, Cheng HB, Wang YW (2007) Removal rate and surface roughness in the lapping and polishing of RB-SiC optical components. J Mater Process Technol 192:276–280
13. Liu L, Zhang F (2017) Prediction model of form error influenced by grinding wheel wear in grinding process of large-scale aspheric surface with SiC ceramics. Int J Adv Manuf Technol 1(88):899–906
14. Li C, Zhang F, Ma Z, Ding Y (2016) Modeling and experiment of surface error for large-aperture aspheric SiC mirror based on residual height and wheel wear. Int J Adv Manuf Technol. https://doi.org/10.1007/s00170-016-9753-3
15. Liew PJ, Yan J, Kuriyagawa T (2014) Fabrication of deep micro-holes in reaction-bonded SiC by ultrasonic cavitation assisted micro-EDM. Int J Mach Tools Manuf 76:13–20
16. Liew PJ, Yan J, Kuriyagawa T (2013) Experimental investigation on material migration phenomena in micro-EDM of reaction-bonded silicon carbide. Appl Surf Sci 276:731–743
17. Liew PJ, Shimada K, Mizutani M, Yan J, Kuriyagawa T (2013) Fabrication of microstructures on RB-SiC by ultrasonic cavitation assisted micro-electrical discharge machining. Int J Autom Technol 7:621–629
18. Clijsters S, Liu K, Reynaerts D, Lauwers B (2010) EDM technology and strategy development for the manufacturing of complex parts in SiSiC. J Mater Process Technol 210(4):631–641
19. Kato T, Noro T, Takahashi H, Yamaguchi S, Arai K (2009) Characterization of electric discharge machining for silicon carbide single crystal. Trans Tech Publ 600:855–858
20. Luis CJ, Puertas I, Villa G (2005) Material removal rate and electrode wear study on the EDM of silicon carbide. J Mater Process Technol 164:889–896
21. Koshy P, Jain VK, Lal GK (1996) Mechanism of material removal in electrical discharge diamond grinding. Int J Mach Tools Manuf 36(10):1173–1185
22. Choudhury SK, Jain VK, Gupta M (1999) Electrical discharge diamond grinding of high speed steel. Mach Sci Technol 3(1):91–105
23. Koshy P, Jain VK, Lal GK (1997) Grinding of cemented carbide with electrical spark assistance. J Mater Process Technol 72(1): 61–68
24. Wei B, Rajurkar KP (1995) Abrasive electrodischarge grinding of superalloys and ceramics. Technical Papers-Society of Manufacturing Engineers-All Series
25. Satyarthi MK, Pandey PM (2013) Modeling of material removal rate in electric discharge grinding process. Int J Mach Tools Manuf 74:65–73

26. Agrawal SS, Yadava V (2013) Modeling and prediction of material removal rate and surface roughness in surface-electrical discharge diamond grinding process of metal matrix composites. Mater Manuf Process 28(4):381–389
27. Shrivastava PK, Dubey AK (2013) Intelligent modeling and multiobjective optimization of electric discharge diamond grinding. Mater Manuf Process 28(9):1036–1041
28. Singh GK, Yadava V, Kumar R (2010) Diamond face grinding of WC-Co composite with spark assistance: experimental study and parameter optimization. Int J Precis Eng Manuf 11(4):509–518
29. Kumar S, Choudhury SK (2007) Prediction of wear and surface roughness in electro-discharge diamond grinding. J Mater Process Technol 191(1):206–209
30. Li Z, Zhang F, Zhang Y, Luo X (2017) Experimental investigation on the surface and subsurface damages characteristics and formation mechanisms in ultra-precision grinding of SiC. Int J Adv Manuf Technol. https://doi.org/10.1007/s00170-017-0267-4
31. Ji R, Liu Y, Zhang Y, Wang F, Cai B, Dong X (2012) Machining performance optimization in end ED milling and mechanical grinding compound process. Mater Manuf Process 27(2):221–228
32. Zhang JH, Ai X, Lee KW, Wong PK (1996) Study on electro discharge diamond wheel grinding (EDGM) of ceramic materials. Mater Manuf Process 11(5):763–774
33. Ji RJ, Liu YH, Zhang YZ, Wang F, Cai BP, Li H (2012) Compound machining of silicon carbide ceramics by high speed end electrical discharge milling and mechanical grinding. Chin Sci Bull 57(4): 421–434
34. Shu KM, Tu GC (2003) Study of electrical discharge grinding using metal matrix composite electrodes. Int J Mach Tools Manuf 43(8): 845–854
35. Ji R, Liu Y, Zhang Y, Cai B, Li X, Zheng C (2013) Effect of machining parameters on surface integrity of silicon carbide ceramic using end electric discharge milling and mechanical grinding hybrid machining. J Mech Sci Technol 27(1):177–183
36. Kozak J (2002) Abrasive electrodischarge grinding (AEDG) of advanced materials. Arch Civil Mech Eng 2(1):83–101
37. Ono T, Sim DY, Esashi M (2000) Micro-discharge and electric breakdown in a micro-gap. J Micromech Microeng 10(3):445
38. Fengguo C (2014) Electro-discharge machining. Chemical Industry Press, Beijing, pp 26–31
39. Yang X, Guo C, Pei J (2014) Principle and application of electric spark forming. National Defense Industry Press, Beijing, pp 42–67
40. Germer LH (1959) Electrical breakdown between close electrodes in air. J Appl Phys 30(1):46–51
41. Torres JM, Dhariwal RS (1999) Electric field breakdown at micrometre separations. Nanotechnology 10(1):102
42. Zeilmann RP, Bordin FM, Vacaro T (2015) Surface integrity of electrodischarge machined cavities for different depths and radii. J Braz Soc Mech Sci Eng 37(1):93–104
43. Yadava V, Jain VK, Dixit PM (2002) Temperature distribution during electro-discharge abrasive grinding. Mach Sci Technol 6(1):97–127
44. Liu Y, Ji R, Zhang Y, Li X (2015) Electrical discharge machining of insulating and weakly conductive engineering ceramics. Science Press, Beijing, pp 52–69